Neural Computing and Applications (2022) 34:3783–3794
https://doi.org/10.1007/s00521-021-06640-0

ORIGINAL ARTICLE

Radiative and magnetohydrodynamic micropolar hybrid nanofluid flow over a shrinking sheet with Joule heating and viscous dissipation effects

Iskandar Waini[1,2] · **Anuar Ishak**[2] · **Ioan Pop**[3]

Received: 13 April 2021 / Accepted: 15 October 2021 / Published online: 27 October 2021

Abstract

This study examines the radiative and magnetohydrodynamic micropolar fluid flow over a stretching/shrinking sheet consisting of Al_2O_3 and Cu nanoparticles. Besides, the effects of the Joule heating and viscous dissipation are taken into consideration. The similarity variables are employed to convert the governing equations into similarity equations. Then, the bvp4c in MATLAB is utilized to obtain the numerical results. The accuracy of the current formulation and method has been done by comparing the present results with those previously published data. Findings discovered that two solutions are obtained for the limited range of S and K, and these solutions are terminated at $S = S_c$ and $K = K_c$. The influence of Ec and R is to reduce the local Nusselt number of $\mathrm{Re}_x^{-1/2}\mathrm{Nu}_x$. Meanwhile, the values of $\mathrm{Re}_x^{-1/2}\mathrm{Nu}_x$ increase with the increase in φ_{hnf} when larger values of R are considered. The rise of M contributes to the increment in the values of $\mathrm{Re}_x^{1/2}C_f$, $\mathrm{Re}_x M_w$, and $\mathrm{Re}_x^{-1/2}\mathrm{Nu}_x$, but the effect of K lowers the values of these physical quantities. Lastly, it was discovered that the first solution is physically reliable and in a stable mode.

Keywords Heat transfer · Micropolar · Hybrid nanofluid · Shrinking sheet · MHD · Radiation · Viscous dissipation · Joule heating · Dual solutions

1 Introduction

The concept of adding a single type of nanoparticle into the base fluid was initiated by Choi and Eastman [1] in 1995. This mixture is called 'nanofluid' which is believed that it can improve the thermal conductivity of the base fluid. The advantages of nanofluids in a rectangular enclosure have been reported by Khanafer et al. [2], Tiwari and Das [3], and Oztop and Abu-Nada [4]. Several researchers have published papers on nanofluids with various physical aspects, for example, magnetic field [5, 6], viscous dissipation and chemical reaction [7], mixed convection [8], activation energy [9], Dufour and Soret [10], magnetic dipole [11], and velocity slip [12]. Apart from that, the discussion on the fabrication of various nanomaterials using bubble electrospinning is elaborated by He and Liu [13]. Meanwhile, the rheological model of nanoparticles using the two-scale fractal theory is reported by several researchers, see Refs. [14–17].

Besides, this concept has been improved by considering two or more nanoparticles that dispersed simultaneously into the base fluid and called 'hybrid nanofluid'. Hybrid nanofluid is utilized to signal a promising increase in the thermal performance of working fluids since this technology has resulted in a significant change in the design of thermal and cooling systems. As a result of the addition of more types of nanostructures, a fluid with better thermal conductivity has been created. Furthermore, hybrid nanofluids are used in several applications, for example, in

✉ Anuar Ishak
anuar_mi@ukm.edu.my

1 Fakulti Teknologi Kejuruteraan Mekanikal Dan Pembuatan, Universiti Teknikal Malaysia Melaka, Hang Tuah Jaya, 76100 Durian Tunggal, Melaka, Malaysia

2 Department of Mathematical Sciences, Faculty of Science and Technology, Universiti Kebangsaan Malaysia, 43600 UKM Bangi, Selangor, Malaysia

3 Department of Mathematics, Babeş-Bolyai University, 400084 Cluj-Napoca, Romania

the vehicle brake fluid, domestic refrigerator, solar water heating, transformer, and heat exchanger [18]. The earlier experimental works utilizing the hybrid nanoparticles were reported by Turcu et al. [19] and Jana et al. [20]. Besides, Suresh et al. [21] conducted experimental works using Al_2O_3-Cu hybrid nanoparticles to study the enhancement of the fluid thermal conductivity. Besides, the significance of the combination of Al_2O_3 and other nanoparticles was reported by Singh and Sarkar [22] and Farhana et al. [23]. In recent years, hybrid nanofluid is attracting the researcher's attention to study the flow and thermal behaviour, numerically. For instance, the flow in the mini-channel heat sink is done by Kumar and Sarkar [24]. Meanwhile, the flow between two parallel plates with the squeezing effect is reported by Salehi et al. [25]. Moreover, Khashi'ie et al. [26] and Muhammad et al. [27] examined the squeezing flow in a horizontal channel. Apart from that, Waini et al. [28], Khan et al. [29], Zainal et al. [30], and Jamaludin et al. [31] considered the flow towards a shrinking surface.

Most of the processes in manufacturing compromise with the non-Newtonian fluids such as lubricants, paints, biological fluids, polymeric suspensions, and colloidal solutions. In this respect, Eringen [32, 33] has introduced the micropolar theory to describe the microscopic characteristics of these fluids. Since then, many authors have considered micropolar fluid with the effects of various physical parameters like radiation, MHD, viscous dissipation, Joule heating, and chemical reaction as reported in Refs. [34–40]. Moreover, the micropolar nanofluid flow by using Buongiorno [41] nanofluid model has been examined by several researchers, see Refs. [42–48]. Furthermore, the effect of nanoparticles on the micropolar fluid by using the Tiwari and Das [3] nanofluid model with different physical parameters was reported by several researchers. For example, Gangadhar et al. [49] considered the effects of MHD and Newtonian heating, Zaib et al. [50] examined the entropy generation effects, and Souayeh and Alfannakh [51] studied the thermal radiation effects. Moreover, Ghadikolaei et al. [52], Subhani and Nadeem [53, 54], Al-Hanaya et al. [55], Hosseinzadeh et al. [56], Nabwey and Mahdy [57], and Roy et al. [58] reported on the effects of hybrid nanoparticles.

Thus, this paper considers the radiative and MHD micropolar fluid flow over a stretching/shrinking sheet containing Al_2O_3 and Cu nanoparticles. The effects of the Joule heating and the viscous dissipation on the flow behaviour are examined. The dual solutions and their stabilities are also reported in this study.

2 Mathematical formulation

Consider the steady laminar two-dimensional flow of a micropolar fluid over a stretching/shrinking sheet with the hybrid nanoparticles as shown in Fig. 1. The surface velocity is represented by $u_w(x) = ax$ where a is constant. The flow is subjected to the effect of a transverse magnetic field of strength B_0 which is assumed to be applied normally to the surface in the positive y-direction. Also, the radiation, the viscous dissipation, and the Joule heating effects are taken into consideration. Accordingly, the micropolar hybrid nanofluid equations are [34, 36, 37]:

$$\frac{\partial u}{\partial x} + \frac{\partial v}{\partial y} = 0 \tag{1}$$

$$u\frac{\partial u}{\partial x} + v\frac{\partial u}{\partial y} = \left(\frac{\mu_{\mathrm{hnf}} + \kappa}{\rho_{\mathrm{hnf}}}\right)\frac{\partial^2 u}{\partial y^2} + \frac{\kappa}{\rho_{\mathrm{hnf}}}\frac{\partial N}{\partial y} - \frac{\sigma_{\mathrm{hnf}}}{\rho_{\mathrm{hnf}}}B_0^2 u \tag{2}$$

$$u\frac{\partial N}{\partial x} + v\frac{\partial N}{\partial y} = \frac{\omega}{\rho_{\mathrm{hnf}} j}\frac{\partial^2 N}{\partial y^2} - \frac{\kappa}{\rho_{\mathrm{hnf}} j}\left(2N + \frac{\partial u}{\partial y}\right) \tag{3}$$

$$u\frac{\partial T}{\partial x} + v\frac{\partial T}{\partial y} = \frac{1}{(\rho C_p)_{\mathrm{hnf}}}\left(k_{\mathrm{hnf}} + \frac{16\sigma^* T_\infty^3}{3k^*}\right)\frac{\partial^2 T}{\partial y^2} + \frac{1}{(\rho C_p)_{\mathrm{hnf}}}\left[(\mu_{\mathrm{hnf}} + \kappa)\left(\frac{\partial u}{\partial y}\right)^2 + \sigma_{\mathrm{hnf}} B_0^2 u^2\right] \tag{4}$$

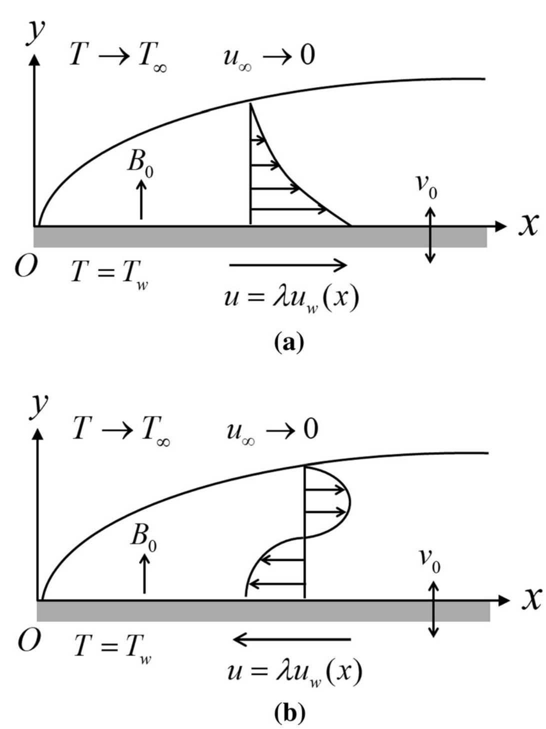

Fig. 1 The flow configuration of **a** stretching and **b** shrinking sheets

subject to:

$$u = \lambda u_w, v = v_0, N = -n\frac{\partial u}{\partial y}, \; T = T_w, \; \text{at} y = 0$$
$$u \to 0, N \to 0, T \to T_\infty \; \text{as} y \to \infty \tag{5}$$

where (u, v) are the corresponding velocity components, N is the microrotation velocity, T is the temperature, κ is the vortex viscosity, n is the micro-gyration parameter, k^* is the mean absorption coefficient, and σ^* is the Stefan–Boltzmann constant. Here, the temperature distribution at the sheet is given by $T_w(x) = T_\infty + T_0(x/L)^2$ with the temperature characteristic T_0, the characteristic length L, and the ambient temperature T_∞. Besides, ω and j are the spin gradient viscosity and the microinertia coefficient, respectively, which are defined as:

$$\omega = \left(\mu_{hnf} + \frac{\kappa}{2}\right)j, \quad j = \frac{\nu_f}{a} \tag{6}$$

Further, the thermophysical properties are obtained from Refs. [59–61] and are given in Tables 1 and 2. Note that the nanoparticles volume fraction is symbolized by φ_1 (Al_2O_3) and φ_2 (Cu). Besides, the subscripts $n1$ and $n2$ are for Al_2O_3 and Cu solid components, whereas f and hnf are for base fluid and the hybrid nanofluid.

Now, following the dimensionless variables [34, 36, 37]:

$$\psi = \sqrt{a\nu_f}\, x f(\eta), N = ax\sqrt{\frac{a}{\nu_f}}g(\eta),$$
$$\theta(\eta) = \frac{T - T_\infty}{T_w - T_\infty}, \eta = y\sqrt{\frac{a}{\nu_f}} \tag{7}$$

with the stream function ψ. Here, $u = \partial\psi/\partial y$ and $v = -\partial\psi/\partial x$, then:

$$u = axf'(\eta), v = -\sqrt{a\nu_f}f(\eta) \tag{8}$$

On using Eqs. (7) and (8), the continuity equation, i.e., Equation (1) is satisfied. Thus, Eqs. (2)–(4) are transformed to:

Table 1 Thermophysical properties of nanoparticles and water [59–61]

Properties	Nanoparticles		Base fluid
	Cu	Al_2O_3	Water
$\rho(kg/m^3)$	8933	3970	997.1
$C_p(J/kgK)$	385	765	4179
$k(W/mK)$	400	40	0.613
$\sigma(S/m)$	5.96×10^7	3.69×10^7	0.05
Prandtl number, Pr			6.2

$$\frac{1}{\rho_{hnf}/\rho_f}\left(\frac{\mu_{hnf}}{\mu_f} + K\right)f''' + ff'' - f'^2 + \frac{K}{\rho_{hnf}/\rho_f}g' - \frac{\sigma_{hnf}/\sigma_f}{\rho_{hnf}/\rho_f}Mf' = 0 \tag{9}$$

$$\frac{1}{\rho_{hnf}/\rho_f}\left(\frac{\mu_{hnf}}{\mu_f} + \frac{K}{2}\right)g'' + fg' - f'g - \frac{K}{\rho_{hnf}/\rho_f}(2g + f'') = 0 \tag{10}$$

$$\frac{1}{\Pr}\frac{1}{(\rho C_p)_{hnf}/(\rho C_p)_f}\left(\frac{k_{hnf}}{k_f} + \frac{4}{3}R\right)\theta'' + f\theta' - 2f'\theta + \frac{\mathrm{Ec}}{(\rho C_p)_{hnf}/(\rho C_p)_f}\left[\left(\frac{\mu_{hnf}}{\mu_f} + K\right)f''^2 + \frac{\sigma_{hnf}}{\sigma_f}Mf'^2\right] = 0 \tag{11}$$

subject to:

$$f(0) = S, f'(0) = \lambda, g(0) = -nf''(0), \theta(0) = 1,$$
$$f'(\eta) \to 0, g(\eta) \to 0, \theta(\eta) \to 0 \text{ as } \eta \to \infty \tag{12}$$

The physical parameters in Eqs. (9)–(12) are the material or micropolar parameter K which provides the ratio of the vortex and the dynamic viscosities, the magnetic parameter M, the Prandtl number Pr, Eckert number Ec c, the radiation parameter R, and the mass flux velocity parameter S, defined as:

$$K = \frac{\kappa}{\mu_f}, M = \frac{\sigma_f B_0^2}{a\rho_f}, \; \Pr = \frac{(\mu C_p)_f}{k_f}, Ec = \frac{a^2L^2}{(C_p)_f T_0},$$
$$R = \frac{4\sigma^* T_\infty^3}{k^* k_f}, S = -\frac{v_0}{\sqrt{a\nu_f}} \tag{13}$$

Note that, $S > 0$ for suction and $S < 0$ for injection. Besides, λ is the stretching/shrinking parameter with $\lambda = 0$ is for the static sheet, whereas $\lambda > 0$ and $\lambda < 0$ are for the stretching and shrinking sheets.

The skin friction coefficient C_f, local couple stress M_w, and local Nusselt number Nu_x are expressed as [46, 62]:

$$C_f = \frac{1}{\rho_f u_w^2}\left((\mu_{hnf} + \kappa)\frac{\partial u}{\partial y} + \kappa N\right)_{y=0}, M_w = \frac{1}{\rho_f x u_w^2}\left(\mu_{hnf} + \frac{\kappa}{2}\right)j\left(\frac{\partial N}{\partial y}\right)_{y=0},$$

$$\mathrm{Nu}_x = -\frac{x}{k_f(T_w - T_\infty)}\left(k_{hnf} + \frac{16\sigma^* T_\infty^3}{3k^*}\right)\left(\frac{\partial T}{\partial y}\right)_{y=0} \tag{14}$$

Table 2 Thermophysical properties of hybrid nanofluid [59–61]

Properties	Correlations
Dynamic viscosity	$\mu_{\text{hnf}} = \frac{\mu_f}{(1-\varphi_{\text{hnf}})^{2.5}}$
Density	$\rho_{\text{hnf}} = (1-\varphi_{\text{hnf}})\rho_f + \varphi_1\rho_{n1} + \varphi_2\rho_{n2}$
Heat capacity	$(\rho C_p)_{\text{hnf}} = (1-\varphi_{\text{hnf}})(\rho C_p)_f + \varphi_1(\rho C_p)_{n1} + \varphi_2(\rho C_p)_{n2}$
Thermal conductivity	$\frac{k_{\text{hnf}}}{k_f} = \frac{\frac{\varphi_1 k_{n1}+\varphi_2 k_{n2}}{\varphi_{\text{hnf}}}+2k_f+2(\varphi_1 k_{n1}+\varphi_2 k_{n2})-2\varphi_{\text{hnf}}k_f}{\frac{\varphi_1 k_{n1}+\varphi_2 k_{n2}}{\varphi_{\text{hnf}}}+2k_f-(\varphi_1 k_{n1}+\varphi_2 k_{n2})+\varphi_{\text{hnf}}k_f}$
Electrical conductivity	$\frac{\sigma_{\text{hnf}}}{\sigma_f} = \frac{\frac{\varphi_1 \sigma_{n1}+\varphi_2 \sigma_{n2}}{\varphi_{\text{hnf}}}+2\sigma_f+2(\varphi_1 \sigma_{n1}+\varphi_2 \sigma_{n2})-2\varphi_{\text{hnf}}\sigma_f}{\frac{\varphi_1 \sigma_{n1}+\varphi_2 \sigma_{n2}}{\varphi_{\text{hnf}}}+2\sigma_f-(\varphi_1 \sigma_{n1}+\varphi_2 \sigma_{n2})+\varphi_{\text{hnf}}\sigma_f}$

Using Eqs. (7) and (14), one gets:

$$\text{Re}_x^{1/2}C_f = \left(\frac{\mu_{\text{hnf}}}{\mu_f} + (1-n)K\right)f''(0),$$
$$\text{Re}_x M_w = \left(\frac{\mu_{\text{hnf}}}{\mu_f} + \frac{K}{2}\right)g'(0)$$
$$\text{Re}_x^{-1/2}\text{Nu}_x = -\left(\frac{k_{\text{hnf}}}{k_f} + \frac{4}{3}R\right)\theta'(0) \tag{15}$$

with the local Reynolds number, $\text{Re}_x = u_w x/\nu_f$.

Moreover, by taking $\varphi_1 = \varphi_2 = M = 0$, and $n = 0.5$, Eq. (9) has the exact solution, see [35, 36]:

$$f(\eta) = S - \frac{2+K}{S \pm \sqrt{S^2-2K-4}}\left[1 - \exp\left(-\frac{S \pm \sqrt{S^2-2K-4}}{2+K}\eta\right)\right] \tag{16}$$

Then,

$$f''(0) = \frac{S \pm \sqrt{S^2-2K-4}}{2+K} \tag{17}$$

Therefore, the comparison values of $f''(0)$ between the present numerical solution and the exact solution (17) can be done for validation purposes.

3 Stability analysis

Here, the temporal stability is conducted by referring to Merkin [63] and Weidman et al. [64]. In this regard, the unsteady form of Eqs. (2)–(4) and the similarity variables as given in Eq. (18) are considered. Therefore,

$$\psi = \sqrt{a\nu_f}\,x f(\eta,\tau), N = ax\sqrt{\frac{a}{\nu_f}}g(\eta,\tau),$$
$$\theta(\eta,\tau) = \frac{T-T_\infty}{T_w-T_\infty}, \eta = y\sqrt{\frac{a}{\nu_f}}, \tau = at \tag{18}$$

where τ is the dimensionless time variable. Then

$$u = ax\frac{\partial f}{\partial \eta}(\eta,\tau), v = -\sqrt{a\nu_f}f(\eta,\tau) \tag{19}$$

On using Eqs. (18) and (19), one obtains

$$\frac{1}{\rho_{\text{hnf}}/\rho_f}\left(\frac{\mu_{\text{hnf}}}{\mu_f} + K\right)\frac{\partial^3 f}{\partial \eta^3} + f\frac{\partial^2 f}{\partial \eta^2} - \left(\frac{\partial f}{\partial \eta}\right)^2 + \frac{K}{\rho_{\text{hnf}}/\rho_f}\frac{\partial g}{\partial \eta} - \frac{\sigma_{\text{hnf}}/\sigma_f}{\rho_{\text{hnf}}/\rho_f}M\frac{\partial f}{\partial \eta} - \frac{\partial^2 f}{\partial \eta \partial \tau} = 0 \tag{20}$$

$$\frac{1}{\rho_{\text{hnf}}/\rho_f}\left(\frac{\mu_{\text{hnf}}}{\mu_f} + \frac{K}{2}\right)\frac{\partial^2 g}{\partial \eta^2} + f\frac{\partial g}{\partial \eta} - \frac{\partial f}{\partial \eta}g - \frac{K}{\rho_{\text{hnf}}/\rho_f}\left(2g + \frac{\partial^2 f}{\partial \eta^2}\right) - \frac{\partial g}{\partial \tau} = 0 \tag{21}$$

$$\frac{1}{\Pr}\frac{1}{(\rho C_p)_{\text{hnf}}/(\rho C_p)_f}\left(\frac{k_{\text{hnf}}}{k_f} + \frac{4}{3}R\right)\frac{\partial^2 \theta}{\partial \eta^2} + f\frac{\partial \theta}{\partial \eta} - 2\frac{\partial f}{\partial \eta}\theta + \frac{Ec}{(\rho C_p)_{\text{hnf}}/(\rho C_p)_f}\left[\left(\frac{\mu_{\text{hnf}}}{\mu_f} + K\right)\left(\frac{\partial^2 f}{\partial \eta^2}\right)^2 + \frac{\sigma_{\text{hnf}}}{\sigma_f}M\left(\frac{\partial f}{\partial \eta}\right)^2\right] - \frac{\partial \theta}{\partial \tau} = 0 \tag{22}$$

subject to:

$$f(0,\tau) = S, \frac{\partial f}{\partial \eta}(0,\tau) = \lambda, g(0,\tau) = -n\frac{\partial^2 f}{\partial \eta^2}(0,\tau), \theta(0,\tau) = 1,$$
$$\frac{\partial f}{\partial \eta}(\eta,\tau) \to 0, g(\eta,\tau) \to 0, \theta(\eta,\tau) \to 0 \text{ as} \eta \to \infty \tag{23}$$

Then, the disturbance is applied to the steady solution $f = f_0(\eta)$, $g = g_0(\eta)$, and $\theta = \theta_0(\eta)$, of Eqs. (9–12) by employing the following relations [64]:

$$f(\eta,\tau) = f_0(\eta) + e^{-\gamma\tau}F(\eta,\tau), g(\eta,\tau) = g_0(\eta) + e^{-\gamma\tau}G(\eta,\tau),$$

$$\theta(\eta,\tau) = \theta_0(\eta) + e^{-\gamma\tau} H(\eta,\tau) \tag{24}$$

Here Eq. (24) is employed to obtain the eigenvalue problems of Eqs. (20)-(23) where $F(\eta,\tau)$,$G(\eta,\tau)$, and $H(\eta,\tau)$ are relatively small compared to $f_0(\eta)$, $g_0(\eta)$, and $\theta_0(\eta)$. After linearization and by setting $\tau = 0$, then $F(\eta,\tau) = F_0(\eta)$, $G(\eta,\tau) = G_0(\eta)$, and $H(\eta,\tau) = H_0(\eta)$. Therefore, the final form of the linearized eigenvalue problems is:

$$\begin{aligned} &\frac{1}{\rho_{hnf}/\rho_f}\left(\frac{\mu_{hnf}}{\mu_f} + K\right)F_0''' + f_0F_0'' + f_0''F_0 - 2f_0'F_0' \\ &+ \frac{K}{\rho_{hnf}/\rho_f}G_0' - \frac{\sigma_{hnf}/\sigma_f}{\rho_{hnf}/\rho_f}MF_0' + \gamma F_0' \\ &= 0 \end{aligned} \tag{25}$$

$$\begin{aligned} &\frac{1}{\rho_{\mathrm{hnf}}/\rho_f}\left(\frac{\mu_{\mathrm{hnf}}}{\mu_f} + \frac{K}{2}\right)G_0'' + f_0G_0' + g_0'F_0 - f_0'G_0 - g_0F_0' \\ &- \frac{K}{\rho_{\mathrm{hnf}}/\rho_f}\left(2G_0 + F_0''\right) + \gamma G_0 \\ &= 0 \end{aligned} \tag{26}$$

$$\begin{aligned} &\frac{1}{\Pr}\frac{1}{(\rho C_p)_{\mathrm{hnf}}/(\rho C_p)_f}\left(\frac{k_{\mathrm{hnf}}}{k_f} + \frac{4}{3}R\right)H_0'' + f_0H_0' + \theta_0'F_0 \\ &- 2\left(\theta_0F_0' + f_0'H_0\right) \\ &+ \frac{\mathrm{Ec}}{(\rho C_p)_{\mathrm{hnf}}/(\rho C_p)_f}\left[2\left(\frac{\mu_{\mathrm{hnf}}}{\mu_f} + K\right)f_0''F_0'' + 2\frac{\sigma_{\mathrm{hnf}}}{\sigma_f}\mathrm{M}f_0'F_0'\right] \\ &+ \gamma H_0 \\ &= 0 \end{aligned} \tag{27}$$

subject to:

$$\begin{aligned} &F_0(0) = 0, F_0'(0) = 0, G_0(0) = -nF_0''(0), H_0(0) = 0, \\ &F_0'(\eta) \to 0, G_0(\eta) \to 0, H_0(\eta) \to 0 \ \text{as}\, \eta \to \infty \end{aligned} \tag{28}$$

Here the values of γ from Eqs. (25)–(27) are generated by setting the new boundary condition $F_0''(0) = 1$ in Eq. (28) to replace $F_0'(\eta) \to 0$ as $\eta \to \infty$ [65]. For additional reference, He et al. [66] investigated the interface stability of a system confined between two horizontal rigid planes and saturated porous media. They concluded that further physical parameters in the stability configuration are shown in the numerical calculations. The involvement of the linear/nonlinear curves shows stability is only judged by the linear curve.

4 Results and discussion

This section provides a discussion of the results obtained from the numerical computations. Here, Eqs. (9)–(12) are solved numerically by utilizing the package bvp4c in MATLAB software [67]. Further, the effect of several physical parameters is examined and then presented in tabular and graphical forms. Here, the hybrid nanofluid $(\varphi_{hnf} = \varphi_1 + \varphi_2)$ consists of Al_2O_3 (φ_1) and Cu (φ_2) nanoparticles with one-to-one ratio.

The value of $f''(0)$ and $g'(0)$ when $\varphi_{\mathrm{hnf}} = S = n = 0$ and $\lambda = 1$ (stretching case) for several values of K and M is given in Table 3. These values are compared to those obtained by Hsiao [42] and Atif et al. [37] and found in good agreement. The exact solution for the case $K = 0$ and $\lambda = 1$ (stretching case) is given by

$$f(\eta) = s + \frac{2}{S + \sqrt{S^2 + 4(M+1)}} - \frac{2}{S + \sqrt{S^2 + 4(M+1)}} \exp\left(-\frac{S + \sqrt{S^2 + 4(M+1)}}{2}\eta\right) \tag{29}$$

which yields $f''(0) = -\frac{S+\sqrt{S^2+4(M+1)}}{2}$. By substituting $s = 0$ and $M = 1$ for example, one obtains $f''(0) = -\sqrt{2} \approx -1.414214$, as shown in Table 3. Moreover, when $s = 0$ and $M = 0$, Eq. (29) reduces to $f(\eta) = 1 - \exp(-\eta)$, which was first reported by Crane [68].

Table 4 provides the values of $f''(0)$ when $\varphi_{\mathrm{hnf}} = M = 0$, $n = 0.5$, and $\lambda = -1$ (shrinking case) for various values of K and S. The present results are validated with the exact solution given in Eq. (17) and also with Lund et al. [36]. Here, the numerical values of the exact solution are approximately taken in six decimal places. The comparisons show an excellent agreement and consequently give us confidence in the validity and accuracy of the present numerical results.

Besides, Table 5 shows the effect of various parameters on $\mathrm{Re}_x^{1/2}C_f$, Re_xM_w, and $\mathrm{Re}_x^{-1/2}\mathrm{Nu}_x$ when $\lambda = -1$, $S = 2$, $n = 0.5$, and $\Pr = 6.2$. Some of the physical parameters such as φ_{hnf}, M, and K have a direct impact on these physical quantities. The values of $\mathrm{Re}_x^{1/2}C_f$, Re_xM_w, and $\mathrm{Re}_x^{-1/2}\mathrm{Nu}_x$ are enhanced with the rise of φ_{hnf} and M, but their values are decreased as K increases. However, no changes are observed in the values of $\mathrm{Re}_x^{1/2}C_f$ and Re_xM_w for Ec and R, whereas the values of $\mathrm{Re}_x^{-1/2}\mathrm{Nu}_x$ are decreased with these parameters.

Further, Fig. 2 is provided to have a better insight into the effect of Ec, R, and φ_{hnf} on $\mathrm{Re}_x^{-1/2}\mathrm{Nu}_x$ when $\lambda = -1, S = 2, K = M = 0.1, n = 0.5$, and $\Pr = 6.2$. A reduction in the values of $\mathrm{Re}_x^{-1/2}\mathrm{Nu}_x$ on the first solution is

Table 3 Values of $f''(0)$ and $g'(0)$ when $\varphi_{\mathrm{hnf}} = S = n = 0$ and $\lambda = 1$ (stretching case)

K	M	Present results		Hsiao [42]		Atif et al. [37]	
		$f''(0)$	$g'(0)$	$f''(0)$	$g'(0)$	$f''(0)$	$g'(0)$
0	1	−1.414214	0	−1.4142	0	−1.414216	0
0.5		−1.140766	0.211167	−1.1408	0.2112	−1.140786	0.211162
2		−0.769666	0.358554	−0.7697	0.3586	−0.769758	0.358664
0.2	0	−0.909737	0.094997	−0.9098	0.0950	−0.909830	0.095017
	0.5	−1.114375	0.105090	−1.1147	0.1051	−1.114379	0.100854
	1	−1.287135	0.112126	−1.2871	0.1121	−1.287136	0.112121

Table 4 Values of $f''(0)$ when $\varphi_{hnf} = M = 0$, $n = 0.5$ and $\lambda = -1$ (shrinking case)

K	S	First solution			Second solution		
		Present results	Equation (17)	Lund et al. [36]	Present results	Equation (17)	Lund et al. [36]
0	2	1.000016	1	1.00009998	–	–	–
	2.5	2.000000	2	1.99999999	0.500000	0.5	0.49710246
0.1	3	2.471852	2.471852	2.47185249	0.385290	0.385290	0.38486773
	3.5	3.017739	3.017739	3.01773913	0.315594	0.315594	0.31386568
0.5	3	2.000000	2	2.00000000	0.400000	0.4	0.39990306
	3.5	2.477033	2.477033	2.47703306	0.322967	0.322967	0.31959198

Table 5 Values of $\mathrm{Re}_x^{1/2} C_f$, $\mathrm{Re}_x M_w$, and $\mathrm{Re}_x^{-1/2}\mathrm{Nu}_x$ when $\lambda = -1$, $S = 2$, $n = 0.5$, and $\mathrm{Pr} = 6.2$

$\varphi_{\mathrm{hnf}}(\%)$	M	K	Ec	R	$\mathrm{Re}_x^{1/2} C_f$	$\mathrm{Re}_x M_w$	$\mathrm{Re}_x^{-1/2}\mathrm{Nu}_x$
0	0.1	0.1	0.1	1	1.238128	0.668140	7.639184
1					1.355528	0.791492	7.680372
2					1.465554	0.910678	7.689165
2	0				1.201237	0.654821	7.289385
	0.03				1.319614	0.770165	7.503985
	0.05				1.369942	0.818765	7.575723
	0.1	0			1.528360	1.041076	7.909083
		0.03			1.510556	1.001801	7.846124
		0.05			1.498231	0.975732	7.802870
		0.1	0 s		1.465554	0.910678	8.478045
			0.03		1.465554	0.910678	8.241381
			0.05		1.465554	0.910678	8.083605
			0.1	0	1.465554	0.910678	9.864474
				0.3	1.465554	0.910678	9.203652
				0.5	1.465554	0.910678	8.763163

observed with the rise of Ec and R. Meanwhile, it is noticed that an increase in φ_{hnf} led to a decrease in the values of $\mathrm{Re}_x^{-1/2}\mathrm{Nu}_x$ for smaller values of R. However, the values of $\mathrm{Re}_x^{-1/2} Nu_x$ start to boost up as φ_{hnf} increases when R becomes large. From these observations, R and φ_{hnf} can be the control parameters to enhance or reduce the heat transfer rate.

Next, the variations of $\mathrm{Re}_x^{1/2} C_f$, $\mathrm{Re}_x M_w$, and $\mathrm{Re}_x^{-1/2}\mathrm{Nu}_x$ against S for $\varphi_{\mathrm{hnf}} = 0\%, 1\%$, and 2% when $\lambda = -1, n = 0.5$, $K = M = Ec = 0.1, R = 1$, and $\mathrm{Pr} = 6.2$ are presented in Figs. 3–5, respectively. It can be concluded from these figures that the values of $\mathrm{Re}_x^{1/2} C_f$, $\mathrm{Re}_x M_w$, and $\mathrm{Re}_x^{-1/2}\mathrm{Nu}_x$ on the first solution are higher for hybrid nanofluid with a volume fraction of 2% ($\varphi_{\mathrm{hnf}} = 2\%$) compared to water ($\varphi_{hnf} = 0\%$). Besides, two solutions are

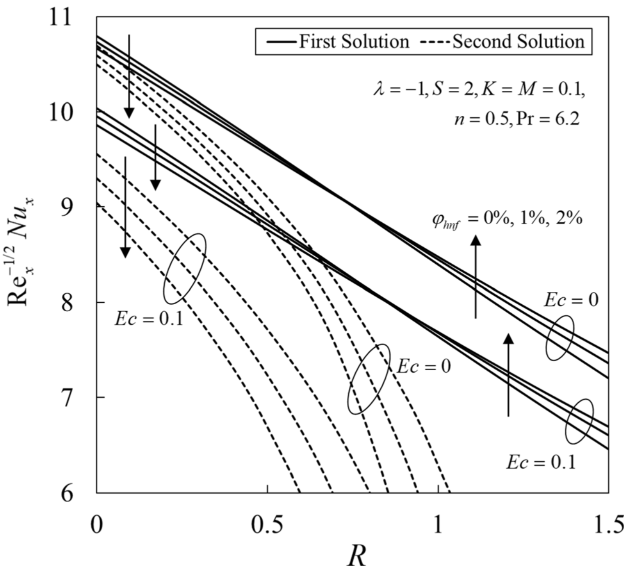

Fig. 2 Variations of $\mathrm{Re}_x^{-1/2}\mathrm{Nu}_x$ for various values of R, Ec and φ_{hnf}

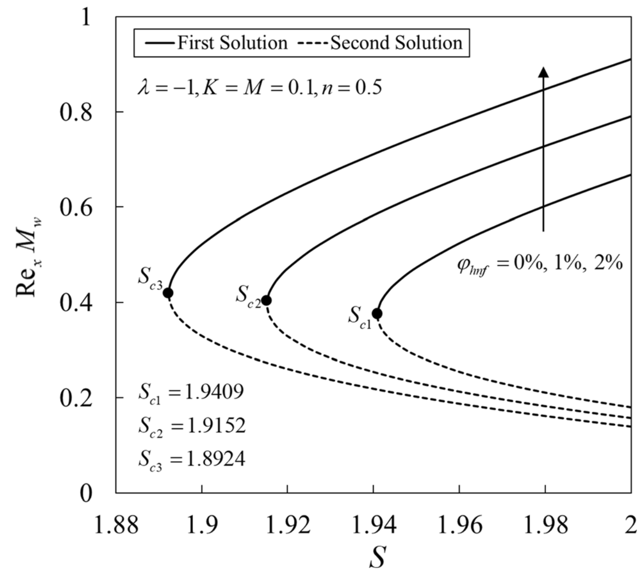

Fig. 4 Variations of $\mathrm{Re}_x M_w$ for various values of S and φ_{hnf}

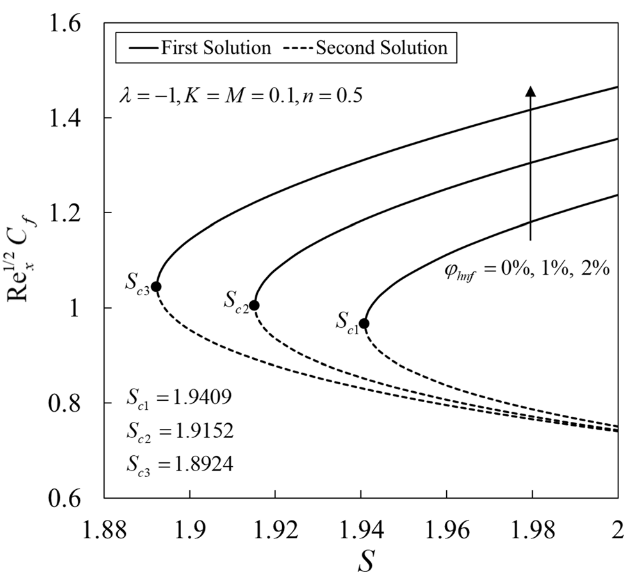

Fig. 3 Variations of $\mathrm{Re}_x^{1/2}C_f$ for various values of S and φ_{hnf}

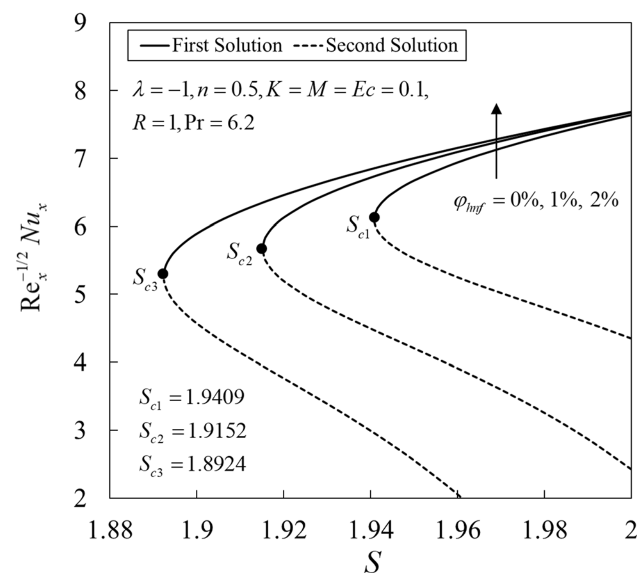

Fig. 5 Variations of $\mathrm{Re}_x^{-1/2}Nu_x$ for various values of S and φ_{hnf}

observed for the limited range of S and these solutions are terminated at $S=S_c$ (critical value). Here, the critical values are $S_{c1}=1.9409$, $S_{c2}=1.9152$, and $S_{c3}=1.8924$ for $\varphi_{\mathrm{hnf}}=0\%, 1\%$, and 2%, respectively.

The effects of M and K on $\mathrm{Re}_x^{1/2}C_f$, $\mathrm{Re}_x M_w$, and $\mathrm{Re}_x^{-1/2}\mathrm{Nu}_x$ when $\lambda=-1, S=2, n=0.5, Ec=0.1, R=1, \Pr=6.2$, and $\varphi_{\mathrm{hnf}}=2\%$ are given in Figs. 6–8, respectively. It is noticed that the values of $\mathrm{Re}_x^{1/2}C_f$, $\mathrm{Re}_x M_w$, and $\mathrm{Re}_x^{-1/2}\mathrm{Nu}_x$ are lower in the absence of the magnetic field ($M=0$). Moreover, the values of these physical quantities are boosted when a stronger magnetic field is applied to the flow. Besides, an increase in K declines the values of $\mathrm{Re}_x^{1/2}C_f$, $\mathrm{Re}_x M_w$, and $\mathrm{Re}_x^{-1/2}\mathrm{Nu}_x$. Interestingly, it is noticed that the solutions only exist up to certain values of K with $K_{c1}=0.1152$, $K_{c2}=0.2327$, and $K_{c3}=0.3649$ for $M=0, 0.05$, and 0.1.

Furthermore, the influence of K on the velocity $f'(\eta)$, the microrotation $g(\eta)$, and the temperature $\theta(\eta)$ profiles when $\lambda=-1, S=2, n=0.5, M=0.05, Ec=0.1, R=1, \Pr=6.2$, and $\varphi_{\mathrm{hnf}}=2\%$ is presented in Figs. 9, 10, and 11. There exist dual solutions on these profiles that satisfy the infinity boundary conditions (12) asymptotically. These solutions are merging up to certain values of K and terminated at $K=K_c$, as evidently shown in Figs. 6, 7, and 8. Besides, it can be seen in Figs. 9 and 10 that the values of

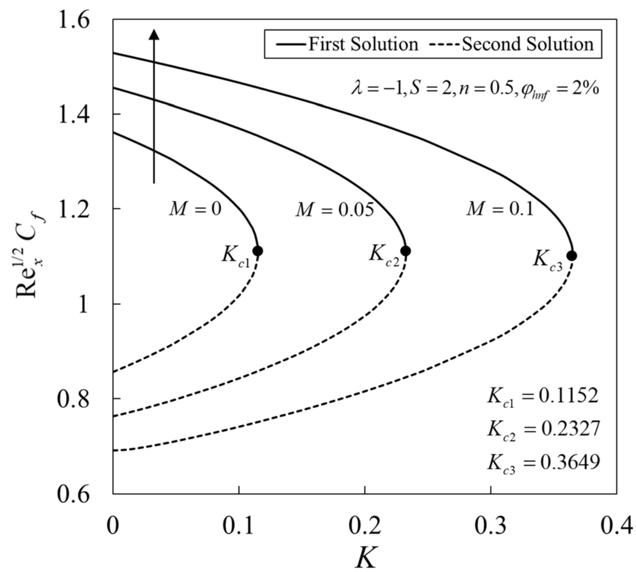

Fig. 6 Variations of $\mathrm{Re}_x^{1/2} C_f$ for various values of K and M

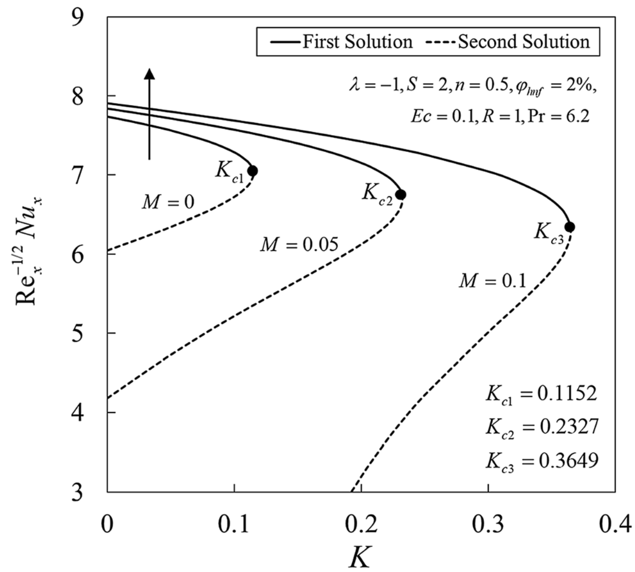

Fig. 8 Variations of $\mathrm{Re}_x^{-1/2}\mathrm{Nu}_x$ for various values of K and M

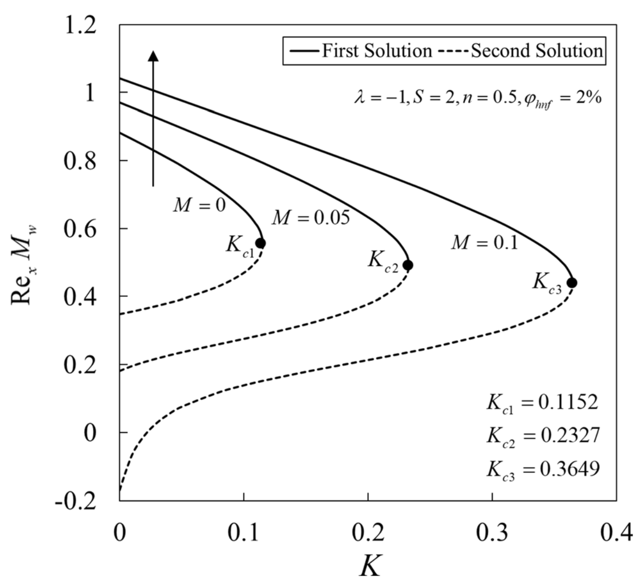

Fig. 7 Variations of $\mathrm{Re}_x M_w$ for various values of K and M

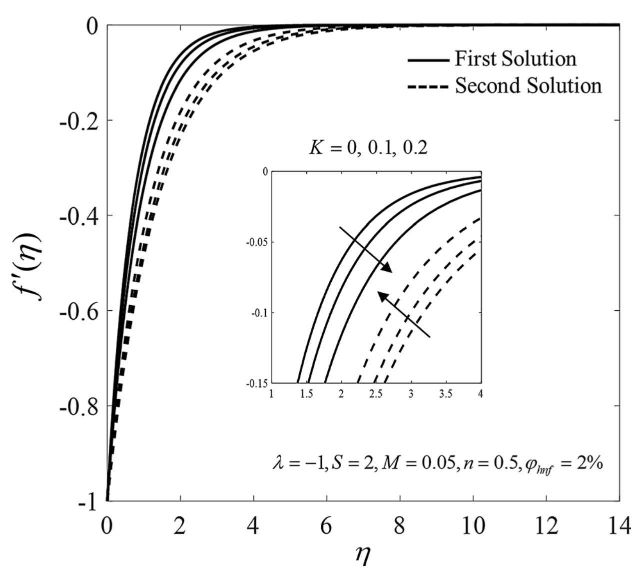

Fig. 9 Velocity profiles $f'(\eta)$ for various values of K

$f'(\eta)$ and $g(\eta)$ on the first solution are declined for larger K. Physically, the micropolarity is neglected when $K=0$. The effect of the vortex and the dynamic viscosities takes place as K increases and consequently raises the momentum boundary layer thickness. Similar observations are reported by several researchers such as Ishak et al. [69], Yacob and Ishak [70], and Soid et al. [71]. Contrarily, the observations are reversed for $\theta(\eta)$ as shown in Fig. 11.

The flow patterns can be determined by plotting the dimensionless stream functions given in Eq. (7) where $\overline{\psi}=\psi/\sqrt{a\nu_f}$. In this respect, the streamlines of the first and the second solutions for the shrinking sheet ($\lambda=-1$) when $S=2$ (suction), $n=0.5, K=M=0.1$, and $\varphi_{\mathrm{hnf}}=2\%$ are shown in Figs. 12 and 13, respectively. It is noticed that the fluid is shrunk towards the slot ($x=0$) on both solution branches and consequently sucked through the surface. Meanwhile, the effect of different S on the flow patterns for the stretching sheet ($\lambda=1$) when $n=0.5, K=M=0.1$, and $\varphi_{\mathrm{hnf}}=2\%$ are shown in Figs. 14, 15, and 16. For $S=0.5$ (suction case), the fluid stretches away from the slot ($x=0$) and being sucked into the surface. Meanwhile, the flow is moving away from the slot for $S=0$ (impermeable case) and $S=-0.5$ (injection case). Also, it is noted that the flow acts as the normal stagnation point flow for $S=0$ (impermeable case) and the flow is split into two regions for $S=-0.5$ (injection case).

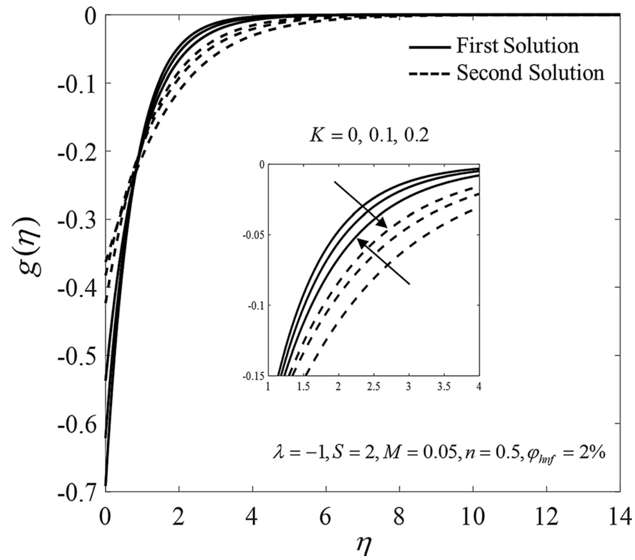

Fig. 10 Microrotation profiles $g(\eta)$ for various values of K

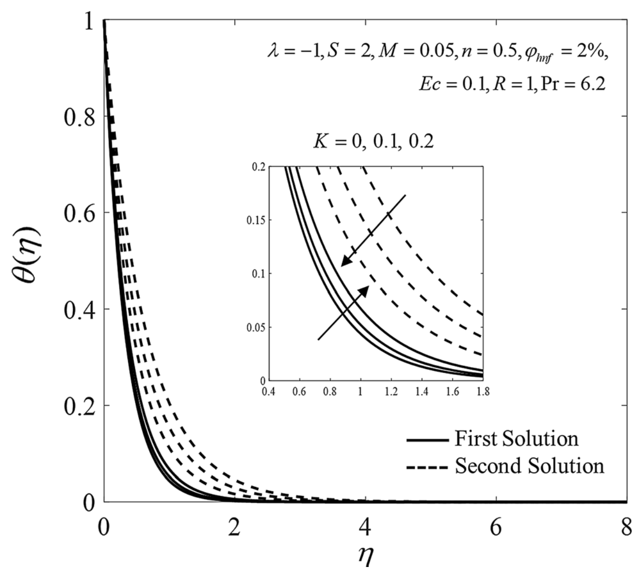

Fig. 11 Temperature profiles $\theta(\eta)$ for various values of K

The variation of γ against S when $\lambda = -1, n = 0.5, K = M = 0.1$, and $\varphi_{\mathrm{hnf}} = 2\%$ is designated in Fig. 17. For the positive value of γ, it is noted that $e^{-\gamma\tau} \rightarrow 0$ as time evolves ($\tau \rightarrow \infty$). For the negative value of γ, $e^{-\gamma\tau} \rightarrow \infty$. As shown in Fig. 17, it is noted that the first solution is stable and vice versa.

5 Conclusion

The radiative and magnetohydrodynamic micropolar fluid flow over a stretching/shrinking sheet consists of Al_2O_3 and Cu nanoparticles with viscous dissipation, and the

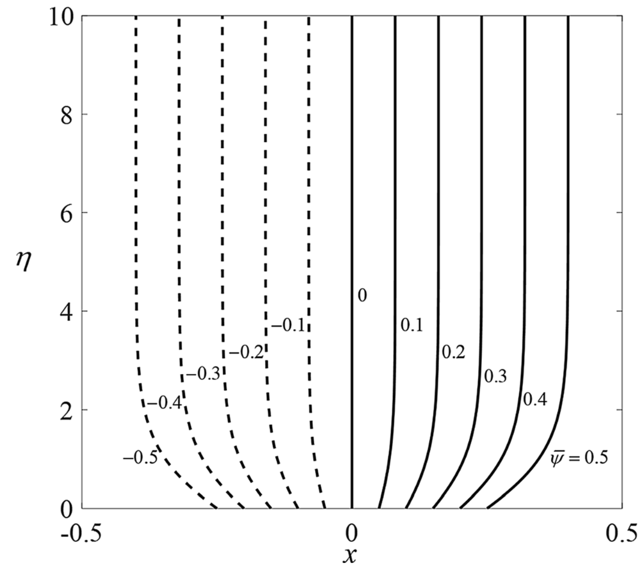

Fig. 12 Streamlines when $\lambda = -1$ (shrinking sheet) for the first solution

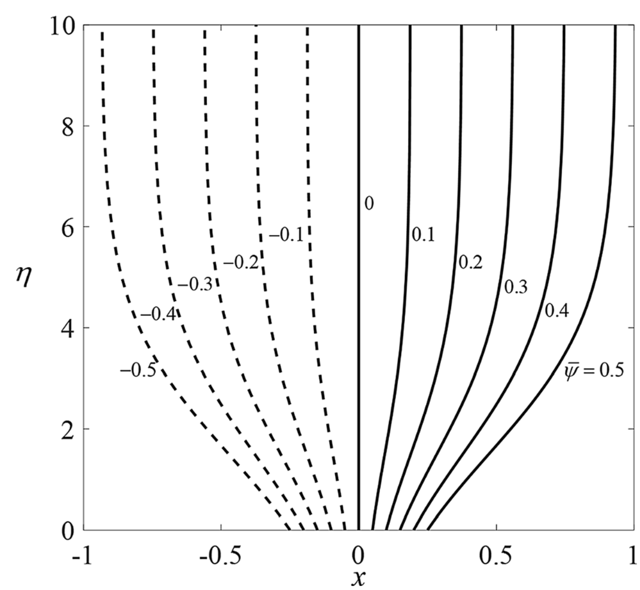

Fig. 13 Streamlines when $\lambda = -1$ (shrinking sheet) for the second solution

Joule heating effect is examined in this paper. The problem is solved numerically with the aid of the bvp4c function. The numerical results are validated with those previously published data to confirm the accuracy of the current formulation and method. Findings reveal that two solutions are possible when a sufficient suction strength is imposed on the shrinking sheet. It is interesting to note that the solutions only exist for a certain range of K. Also, the similarity solutions terminate at $S = S_c$ and $K = K_c$. The values of $\mathrm{Re}_x^{-1/2}\mathrm{Nu}_x$ reduce with the rise of Ec and R.

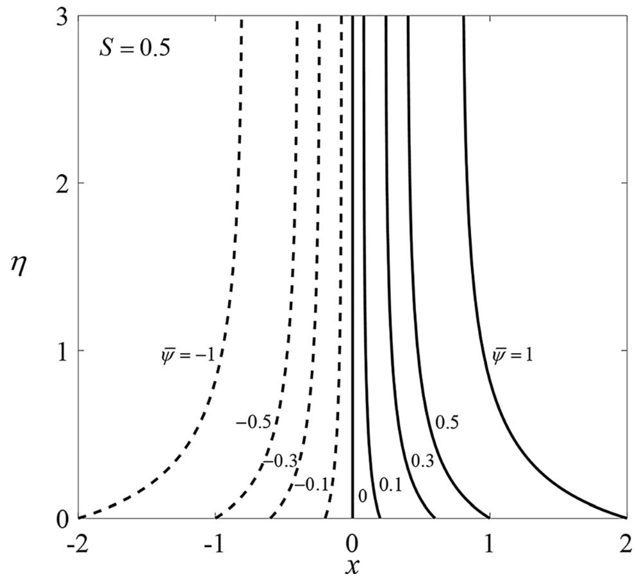

Fig. 14 Streamlines when $\lambda = 1$ (stretching sheet) and $S = 0.5$ (suction)

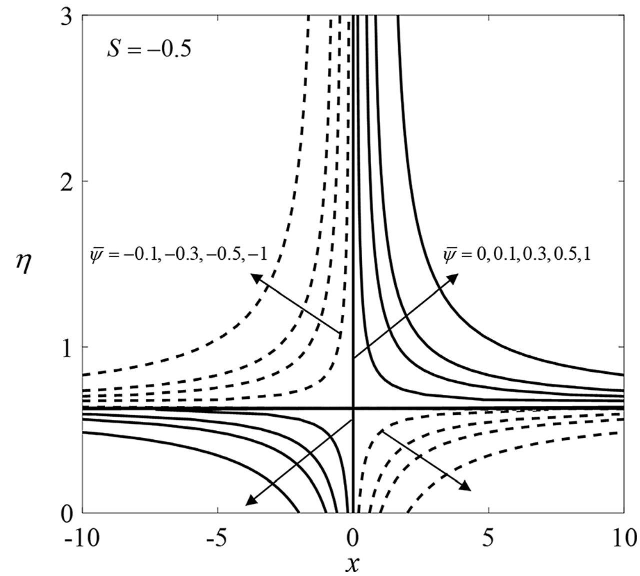

Fig. 16 Streamlines when $\lambda = 1$ (stretching sheet) and $S = -0.5$ (injection)

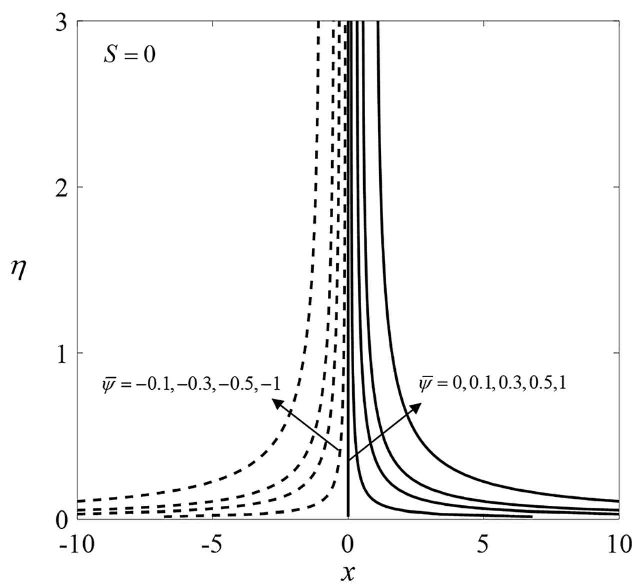

Fig. 15 Streamlines when $\lambda = 1$ (stretching sheet) and $S = 0$ (impermeable)

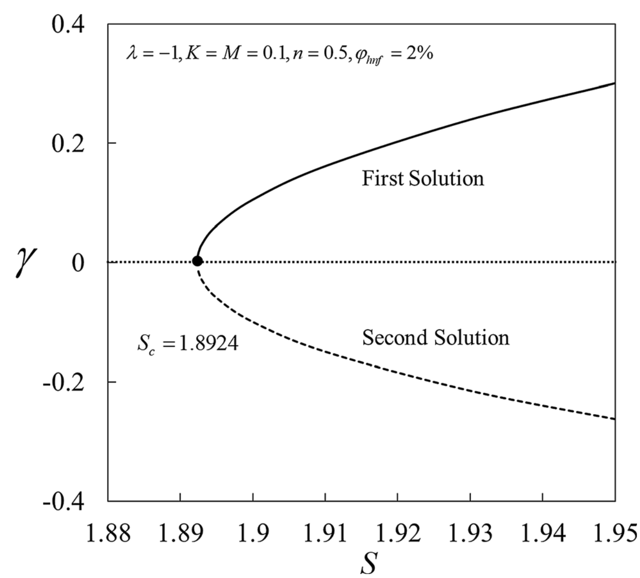

Fig. 17 Eigenvalues γ against S

Besides, an increase in φ_{hnf} leads to a decrease in the values of $\mathrm{Re}_x^{-1/2}\mathrm{Nu}_x$ for smaller values of R. However, the values of $\mathrm{Re}_x^{-1/2}\mathrm{Nu}_x$ increase with the increase in φ_{hnf} for larger values of R. The values of $\mathrm{Re}_x^{1/2}C_f$, $\mathrm{Re}_x M_w$, and $\mathrm{Re}_x^{-1/2}\mathrm{Nu}_x$ intensify with the rise of M. Contrarily, the effect of K lowers the values of these physical quantities. The plots of the streamlines show that the fluid is shrunk towards the slot ($x = 0$) on both solution branches for the shrinking sheet and consequently sucked into the surface. Lastly, it is discovered that the first solution is physically reliable and in a stable mode.

Acknowledgements The financial supports received from the Universiti Kebangsaan Malaysia (Project Code: DIP-2020-001) and the Universiti Teknikal Malaysia Melaka are gratefully acknowledged.

Declarations

Conflict of interest The authors declare that there is no conflict of interest.

References

1. Choi SUS, Eastman JA (1995) Enhancing thermal conductivity of fluids with nanoparticles. Proc 1995 ASME Int Mech Eng Congr Expo FED 231/MD 66:99–105
2. Khanafer K, Vafai K, Lightstone M (2003) Buoyancy-driven heat transfer enhancement in a two-dimensional enclosure utilizing nanofluids. Int J Heat Mass Transf 46:3639–3653
3. Tiwari RK, Das MK (2007) Heat transfer augmentation in a two-sided lid-driven differentially heated square cavity utilizing nanofluids. Int J Heat Mass Transf 50:2002–2018
4. Oztop HF, Abu-Nada E (2008) Numerical study of natural convection in partially heated rectangular enclosures filled with nanofluids. Int J Heat Fluid Flow 29:1326–1336
5. Hamad MAA (2011) Analytical solution of natural convection flow of a nanofluid over a linearly stretching sheet in the presence of magnetic field. Int Commun Heat Mass Transf 38:487–492
6. Jusoh R, Nazar R, Pop I (2019) Magnetohydrodynamic boundary layer flow and heat transfer of nanofluids past a bidirectional exponential permeable stretching/shrinking sheet with viscous dissipation effect. J Heat Transf 141:012406
7. Kameswaran PK, Narayana M, Sibanda P, Murthy PVSN (2012) Hydromagnetic nanofluid flow due to a stretching or shrinking sheet with viscous dissipation and chemical reaction effects. Int J Heat Mass Transf 55:7587–7595
8. Jamaludin A, Nazar R, Pop I (2019) Mixed convection stagnation-point flow of a nanofluid past a permeable stretching/shrinking sheet in the presence of thermal radiation and heat source/sink. Energies 12:788
9. Khan U, Zaib A, Khan I, Nisar KS (2020) Activation energy on MHD flow of titanium alloy (Ti6Al4V) nanoparticle along with a cross flow and streamwise direction with binary chemical reaction and non-linear radiation: dual solutions. J Mater Res Technol 9:188–199
10. Waini I, Ishak A, Pop I (2021) Dufour and Soret effects on Al_2O_3-water nanofluid flow over a moving thin needle: Tiwari and Das model. Int J Numer Methods Heat Fluid Flow 31:766–782
11. Majeed A, Zeeshan A, Hayat T (2019) Analysis of magnetic properties of nanoparticles due to applied magnetic dipole in aqueous medium with momentum slip condition. Neural Comput Appl 31:189–197
12. Ghosh S, Mukhopadhyay S (2020) Stability analysis for model-based study of nanofluid flow over an exponentially shrinking permeable sheet in presence of slip. Neural Comput Appl 32:7201–7211
13. He J-H, Liu Y-P (2020) Bubble electrospinning: patents, promises and challenges. Recent Pat Nanotechnol 14:3
14. Li X, Liu Z, He JH (2020) A fractal two-phase flow model for the fiber motion in a polymer filling process. Fractals 28:2050093
15. Zuo YT, Liu HJ (2021) Fractal approach to mechanical and electrical properties of graphene/sic composites. Facta Univ Ser Mech Eng 19:271–284
16. Zuo Y (2021) Effect of SiC particles on viscosity of 3-D print paste: A fractal rheological model and experimental verification. Therm Sci 25:2405–2409
17. He JH, Qie N, He CH (2021) Solitary waves travelling along an unsmooth boundary. Res Phys 24:104104
18. Sidik NAC, Adamu IM, Jamil MM et al (2016) Recent progress on hybrid nanofluids in heat transfer applications: a comprehensive review. Int Commun Heat Mass Transf 78:68–79
19. Turcu R, Darabont A, Nan A et al (2006) New polypyrrole-multiwall carbon nanotubes hybrid materials. J Optoelectron Adv Mater 8:643–647
20. Jana S, Salehi-Khojin A, Zhong WH (2007) Enhancement of fluid thermal conductivity by the addition of single and hybrid nano-additives. Thermochim Acta 462:45–55
21. Suresh S, Venkitaraj KP, Selvakumar P, Chandrasekar M (2011) Synthesis of Al_2O_3-Cu/water hybrid nanofluids using two step method and its thermo physical properties. Colloids Surf A Physicochem Eng Asp 388:41–48
22. Singh SK, Sarkar J (2018) Energy, exergy and economic assessments of shell and tube condenser using hybrid nanofluid as coolant. Int Commun Heat Mass Transf 98:41–48
23. Farhana K, Kadirgama K, Rahman MM et al (2019) Significance of alumina in nanofluid technology: an overview. J Therm Anal Calorim 138:1107–1126
24. Kumar V, Sarkar J (2020) Particle ratio optimization of Al_2O_3-MWCNT hybrid nanofluid in minichannel heat sink for best hydrothermal performance. Appl Therm Eng 165:114546
25. Salehi S, Nori A, Hosseinzadeh K, Ganji DD (2020) Hydrothermal analysis of MHD squeezing mixture fluid suspended by hybrid nanoparticles between two parallel plates. Case Stud Therm Eng 21:100650
26. Khash'iie NS, Waini I, Arifin NM, Pop I (2021) Unsteady squeezing flow of Cu-Al2O3/water hybrid nanofluid in a horizontal channel with magnetic field. Sci Rep 11:14128
27. Muhammad K, Hayat T, Alsaedi A, Ahmad B (2021) Melting heat transfer in squeezing flow of basefluid (water), nanofluid (CNTs + water) and hybrid nanofluid (CNTs + CuO + water). J Therm Anal Calorim 143:1157–1174
28. Waini I, Ishak A, Pop I (2021) Hybrid nanofluid flow over a permeable non-isothermal shrinking surface. Mathematics 9:538
29. Khan U, Waini I, Ishak A, Pop I (2021) Unsteady hybrid nanofluid flow over a radially permeable shrinking/stretching surface. J Mol Liq 331:115752
30. Zainal NA, Nazar R, Naganthran K, Pop I (2021) Viscous dissipation and MHD hybrid nanofluid flow towards an exponentially stretching/shrinking surface. Neural Comput Appl 33:11285–11295
31. Jamaludin A, Nazar R, Naganthran K, Pop I (2021) Mixed convection hybrid nanofluid flow over an exponentially accelerating surface in a porous media. Neural Comput Appl. https://doi.org/10.1007/s00521-021-06191-4
32. Eringen A (1966) Theory of micropolar fluids. J Math Mech 16:1–18
33. Eringen AC (1972) Theory of thermomicrofluids. J Math Anal Appl 38:480–496
34. Eldabe NT, Ouaf MEM (2006) Chebyshev finite difference method for heat and mass transfer in a hydromagnetic flow of a micropolar fluid past a stretching surface with Ohmic heating and viscous dissipation. Appl Math Comput 177:561–571
35. Turkyilmazoglu M (2014) A note on micropolar fluid flow and heat transfer over a porous shrinking sheet. Int J Heat Mass Transf 72:388–391
36. Lund LA, Omar Z, Khan I et al (2019) Effect of viscous dissipation in heat transfer of MHD flow of micropolar fluid partial slip conditions: dual solutions and stability analysis. Energies 12:1–17
37. Atif SM, Kamran A, Shah S (2021) MHD micropolar nanofluid with non Fourier and non Fick's law. Int Commun Heat Mass Transf 122:105114
38. Mittal AS, Patel HR, Darji RR (2019) Mixed convection micropolar ferrofluid flow with viscous dissipation, joule heating and convective boundary conditions. Int Commun Heat Mass Transf 108:104320
39. Shehzad SA, Reddy MG, VIjayakumari P, Tlili I, (2020) Behavior of ferromagnetic Fe_2SO_4 and titanium alloy Ti6Al4v nanoparticles in micropolar fluid flow. Int Commun Heat Mass Transf 117:104769

40. Singh K, Pandey AK, Kumar M (2021) Numerical solution of micropolar fluid flow via stretchable surface with chemical reaction and melting heat transfer using Keller-Box method. Propuls Power Res 10:194–207
41. Buongiorno J (2006) Convective transport in nanofluids. J Heat Transf 128:240–250
42. Hsiao KL (2017) Micropolar nanofluid flow with MHD and viscous dissipation effects towards a stretching sheet with multimedia feature. Int J Heat Mass Transf 112:983–990
43. Anwar MI, Shafie S, Hayat T et al (2017) Numerical study for MHD stagnation-point flow of a micropolar nanofluid towards a stretching sheet. J Brazilian Soc Mech Sci Eng 39:89–100
44. Hayat T, Khan MI, Waqas M et al (2017) Radiative flow of micropolar nanofluid accounting thermophoresis and Brownian moment. Int J Hydrogen Energy 42:16821–16833
45. Ibrahim W (2017) Passive control of nanoparticle of micropolar fluid past a stretching sheet with nanoparticles, convective boundary condition and second-order slip. Proc Inst Mech Eng Part E J Process Mech Eng 231:704–719
46. Siddiq MK, Rauf A, Shehzad SA et al (2018) Thermally and solutally convective radiation in MHD stagnation point flow of micropolar nanofluid over a shrinking sheet. Alexandria Eng J 57:963–971
47. Kumar B, Seth GS, Nandkeolyar R (2019) Regression model and successive linearization approach to analyse stagnation point micropolar nanofluid flow over a stretching sheet in a porous medium with nonlinear thermal radiation. Phys Scr 94:115211
48. Patel HR, Singh R (2019) Thermophoresis, Brownian motion and non-linear thermal radiation effects on mixed convection MHD micropolar fluid flow due to nonlinear stretched sheet in porous medium with viscous dissipation, joule heating and convective boundary condition. Int Commun Heat Mass Transf 107:68–92
49. Gangadhar K, Kannan T, Jayalakshmi P (2017) Magnetohydrodynamic micropolar nanofluid past a permeable stretching/shrinking sheet with Newtonian heating. J Brazilian Soc Mech Sci Eng 39:4379–4391
50. Zaib A, Khan U, Shah Z et al (2019) Optimization of entropy generation in flow of micropolar mixed convective magnetite (Fe_3O_4) ferroparticle over a vertical plate. Alexandria Eng J 58:1461–1470
51. Souayeh B, Alfannakh H (2021) Radiative melting heat transfer through a micropolar nanoliquid by using Koo and Kleinstreuer model. Eur Phys J Plus 136:75
52. Ghadikolaei SS, Hosseinzadeh K, Hatami M, Ganji DD (2018) MHD boundary layer analysis for micropolar dusty fluid containing hybrid nanoparticles (Cu-Al_2O_3) over a porous medium. J Mol Liq 268:813–823
53. Subhani M, Nadeem S (2019) Numerical analysis of micropolar hybrid nanofluid. Appl Nanosci 9:447–459
54. Subhani M, Nadeem S (2019) Numerical investigation into unsteady magnetohydrodynamics flow of micropolar hybrid nanofluid in porous medium. Phys Scr 94:105220
55. Al-Hanaya AM, Sajid F, Abbas N, Nadeem S (2020) Effect of SWCNT and MWCNT on the flow of micropolar hybrid nanofluid over a curved stretching surface with induced magnetic field. Sci Rep 10:8488
56. Hosseinzadeh K, Roghani S, Asadi A et al (2020) Investigation of micropolar hybrid ferro fluid flow over a vertical plate by considering various base fluid and nanoparticle shape factor. Int J Numer Methods Heat Fluid Flow 31:402–417
57. Nabwey HA, Mahdy A (2021) Transient flow of micropolar dusty hybrid nanofluid loaded with Fe_3O_4-Ag nanoparticles through a porous stretching sheet. Res Phys 21:103777
58. Roy NC, Hossain MA, Pop I (2021) Analysis of dual solutions of unsteady micropolar hybrid nanofluid flow over a stretching/shrinking sheet. J Appl Comput Mech 7:19–33
59. Takabi B, Salehi S (2014) Augmentation of the heat transfer performance of a sinusoidal corrugated enclosure by employing hybrid nanofluid. Adv Mech Eng 6:147059
60. Hussain S, Ahmed SE, Akbar T (2017) Entropy generation analysis in MHD mixed convection of hybrid nanofluid in an open cavity with a horizontal channel containing an adiabatic obstacle. Int J Heat Mass Transf 114:1054–1066
61. Waini I, Ishak A, Pop I (2020) MHD flow and heat transfer of a hybrid nanofluid past a permeable stretching/shrinking wedge. Appl Math Mech (English Ed) 41:507–520
62. Khashi'ie NS, Arifin NM, Nazar R et al (2019) Mixed convective flow and heat transfer of a dual stratified micropolar fluid induced by a permeable stretching/shrinking sheet. Entropy 21:1162
63. Merkin JH (1986) On dual solutions occurring in mixed convection in a porous medium. J Eng Math 20:171–179
64. Weidman PD, Kubitschek DG, Davis AMJ (2006) The effect of transpiration on self-similar boundary layer flow over moving surfaces. Int J Eng Sci 44:730–737
65. Harris SD, Ingham DB, Pop I (2009) Mixed convection boundary-layer flow near the stagnation point on a vertical surface in a porous medium: Brinkman model with slip. Transp Porous Media 77:267–285
66. He JH, Moatimid GM, Mostapha DR (2021) Nonlinear instability of two streaming-superposed magnetic Reiner-Rivlin Fluids by He-Laplace method. J Electroanal Chem 895:115388
67. Shampine LF, Gladwell I, Thompson S (2003) Solving ODEs with MATLAB. Cambridge University Press, Cambridge
68. Crane LJ (1970) Flow past a stretching plate. Z Angew Math Phys 21:645–647
69. Ishak A, Lok YY, Pop I (2010) Stagnation-point flow over a shrinking sheet in a micropolar fluid. Chem Eng Commun 197:1417–1427
70. Yacob NA, Ishak A (2012) Stagnation point flow towards a stretching/shrinking sheet in a micropolar fluid with a convective surface boundary condition. Can J Chem Eng 90:621–626
71. Soid SK, Ishak A, Pop I (2018) MHD stagnation-point flow over a stretching/shrinking sheet in a micropolar fluid with a slip boundary. Sains Malays 47:2907–2916